Microporous and Mesoporous Materials 300 (2020) 110151

Contents lists available at ScienceDirect

Microporous and Mesoporous Materials

journal homepage: http://www.elsevier.com/locate/micromeso

Hydrogen bonding induces dual porous types with microporous and mesoporous covalent organic frameworks based on bicarbazole units

Hesham R. Abuzeid [a], Ahmed F.M. EL-Mahdy [a], Shiao-Wei Kuo [a,b,**]

[a] Department of Materials and Optoelectronic Science, Center of Crystal Research, National Sun Yat-Sen University, Kaohsiung, 80424, Taiwan
[b] Department of Medicinal and Applied Chemistry, Kaohsiung Medical University, Kaohsiung, 807, Taiwan

ARTICLE INFO

Keywords:
Covalent organic framework (COF)
Hydrogen bonding
Kagome structure
CO_2 capture

ABSTRACT

Although the topologies of covalent organic frameworks (COFs) can be controlled mainly by varying the symmetries of the building blocks condensed to form the structures, another approach is to change the structures of blocks but retain the same symmetries. The construction of a single COF featuring pores of different sizes from two symmetrical building blocks remains extremely difficult. In this paper, we report an investigation into the effect of hydrogen bonding on the topological regulation of two-dimensional COFs as a new approach for managing their properties. Our strategy involved introducing pristine and substituted diamine monomers—benzidine (BD) and 1,4-dihydroxybenzidine (DHBD)—into the skeleton of bicarbazole-based COFs. The constructed bicarbazole-based COFs, Cz-BD and Cz-DHBD, were designed using a ($C_2 + C_2$) geometry strategy and synthesized through Schiff-base condensations of bicarbazole-4CHO and the benzidine derivatives. The resulting COFs featured two different topologies: Cz-BD COF possessing a single type of pore having a tetragonal structure, and Cz-DHBD COF possessing a Kagome structure featuring two types of pores (one hexagonal and the other triangular with mesoporous and microporous structure, induced by intramolecular OH···N hydrogen bonding). These COFs exhibited high crystallinity, great thermal stability, and large surface areas, as well as synergistic structural effects and high-performance CO_2 uptake.

1. Introduction

Covalent organic frameworks (COFs) are micro/mesoporous materials synthesized through covalent linking of building blocks composed of light elements into extended two-dimensional (2D) or three-dimensional (3D) frameworks [1]. Motivated by the rapid development of reticular chemistry in field of zeolitic imidazole frameworks (ZIFs) and metal organic frameworks (MOFs) [2–5], COFs have gained considerable attention due to their highly ordered porosities, which make them a great candidate for many practical implementations—for example, in gas storage and separation, catalysis, proton conduction, sensing, luminescence, drug delivery, electronic devices, and energy conversion and storage [2–13]. Many COF structures have been synthesized, commonly with tetragonal and hexagonal structures, but trigonal and Kagome structures are also known [6–17].

Several approaches have been developed to achieve a diversity of COF topologies, including the introduction of monomers with different geometries. For instance, hexagonal COF structures have been generated through the condensation of two or three components of $C_3 + C_2$ symmetry or through the self-condensation of C_2-symmetric monomers [18–24]. Very recently, a hexagonal cage-based crystalline COF was prepared from a 3D C_3-symmetric cage knot and a 2D C_2-symmetric linker [24]. Most of these developed structures have featured only one type of pores in their extended frameworks of sheets. Because regulating the topology of COFs plays an important role in determining their properties, other topologies and structures have also been generated. For example, dual-pore-type COFs having Kagome structures have been synthesized through the condensations of pairs of building blocks possessing $C_2 + D_{2h}$ and $D_{2h} + D_{2h}$ symmetry [25,26]. These COFs possessed two different pore sizes: micropores and mesopores [25–28]. In another example, however, use of building blocks of the same symmetry resulted in a single-pore-type structure, suggesting that the symmetry of the building blocks is not the only factor affecting the topology of the resulting COFs [29].

Another approach toward controlling the topologies of COFs is by changing the structures of the monomers while retaining the same

* Corresponding author. Department of Materials and Optoelectronic Science, Center of Crystal Research, National Sun Yat-Sen University, Kaohsiung, 80424, Taiwan.
E-mail address: kuosw@faculty.nsysu.edu.tw (S.-W. Kuo).

https://doi.org/10.1016/j.micromeso.2020.110151
Received 11 November 2019; Received in revised form 22 February 2020; Accepted 4 March 2020
Available online 7 March 2020

symmetry. For example, the condensations of building blocks having $C_2 + C_2$ symmetries have resulted in the formation of single-pore-type rhombic-shaped frameworks [30–32] as well as dual- and triple-pore-type Kagome structures [33]. While the π-structure of the building block was the main factor determining the final polygon structure, that introduction of asymmetric monomers for the condensations provoked the formation of heterogeneous porous hexagonal structures [34]. Moreover, the crystallinity of Kagome-type COFs has been enhanced through the docking effects of interlayer interactions [35]. Introducing intramolecular hydrogen bonding into a COF framework can improve its crystallinity, porosity, and chemical stability [36]. Thus, COF structures are sensitive to the interactions of their intra- and interlayer forces, suggesting that control over the supramolecular interactions that regulate the topologies of COFs would be a new technique for managing their properties [37,38].

In this context, we developed a tetraformyl building block (Cz-4CHO) as a C_2-symmetric knot and benzidine (BD) and *N*,*N*′-dihydroxybenzidine (DHBD) as C_2-symmetric linkers to investigate the effect of hydrogen bonding on the topology of their resulting COFs (Scheme 1). DHBD is a building block possessing OH units that can form intramolecular hydrogen bonds with the nitrogen atoms in imide linkages, whereas BD cannot. From a topological perspective, we expected that the COFs obtained of the reactions between these monomers both having $C_2 + C_2$ symmetry would result in two possible structures. One would be an orthorhombic structure, characterized by uniform single pores within its framework. The other would be a hexagonal system featuring two kinds of pores: one hexagonal and the other trigonal. Each system could be assigned to a two-layer stacking structure, either eclipsed (AA-stacking) or staggered (AB-stacking). Consequently, four possible structures could possibly be generated from the reactions of Cz-4CHO with BD and DHBD. Thermodynamically, only the product with the lowest energy would result if the differences among the four possible structures were sufficiently large. To validate this behavior, we obtained pore-size distribution patterns and used modeling and simulations to characterize the as-obtained structures, and we tested the resulting two COFs for their ability to capture CO_2.

2. Experimental section

2.1. Materials

Carbazole (96%, Acros), *n*-butyllithium (2.5 M in hexane, Albemarle), BD (98%, Sigma Aldrich), 3,3′-dihydroxybenzidine (99%, Tokyo Chemical Industry), *N*-bromosuccinimide (NBS, 99%, Acros), hydrochloric acid (HCl, Sigma–Aldrich), mesitylene (99%, Acros), potassium permanganate (99%, Showa), acetic acid (99.8%, Sigma–Aldrich), and *n*-formylpiperidine (99%, Alfa Aesar) were used without any further purification. Synthesis of 3,6-Dibromocarbazole (Cz-2Br), 3,3′,6,6′-Tetrabromo-9,9′-bicarbazole (Cz-4Br), and 3,3′,6,6′-Tetraformyl-9,9′-bicarbazole (Cz-4CHO) were described as supporting information (Schemes S1–S3, Figs. S1–S7).

2.2. Synthesis of Cz-BD COF

3,3′,6,6′-Tetraformyl-9,9′-bicarbazole (111 mg, 0.250 mmol) and BD (92.0 mg, 0.500 mmol) dissolved in a mixture of 1,4-dioxane and mesitylene (1:1, v/v; 9 mL) in a Schlenk storage tube under a N_2 atmosphere and then aqueous acetic acid (6 M, 1.0 mL) was added. The suspension was placed in an oven at 120 °C and left undisturbed for 4 days. The precipitate was collected through filtration and washed

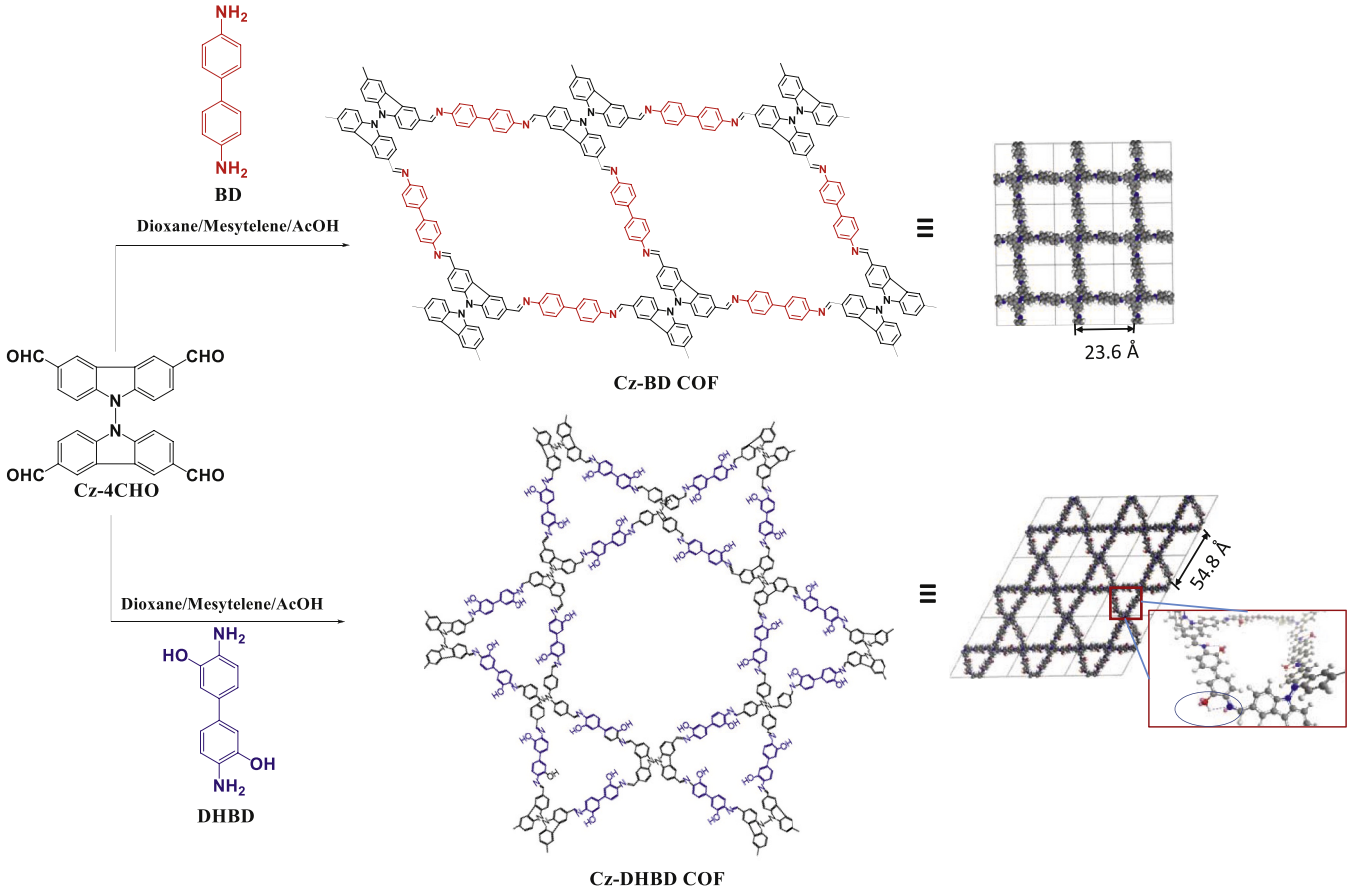

Scheme 1. Synthesis of the Cz-BD and Cz-DHBD COFs.

thoroughly with $CHCl_3$, THF, MeOH, and acetone. The resulting product was dried at 80 °C under vacuum to yield a yellow powder (135 mg, 67%).

2.3. Synthesis of Cz-DHBD COF

Obtained as a dark-yellow powder (135 mg, 67%) from 3,3′,6,6′-tetraformyl-9,9′-bicarbazole (111 mg, 0.250 mmol) and 1,4-dihydroxybenzidine (92.0 mg, 0.500 mmol), in a manner similar to that described above for the Cz-BD COF.

3. Results and discussion

3.1. Synthesis of Cz-BD COF and Cz-HDBD COF

We investigated the effect of using monomers of the same symmetry, but with different structures, on the topologies of their resulting COFs, as well as their porosities, crystallinities, and applications in CO_2 capture. These microporous Cz-COFs were prepared to have $C_2 + C_2$ symmetries, synthesized through Schiff-base condensations of the bicarbazole-based tetraformyl monomer Cz-4CHO and the two aromatic diamines BD and DHBD (Scheme 1). Geometry optimization of the monomer structures using the B3LYP/6-311G(d,p) basis set in Gaussian revealed that all three were nonplanar; Cz-4CHO was extended in two perpendicular positions with a torsional angle of 125°; similarly, BD and DHBD both featured almost the same torsional angle of 125.5°. Fig. 1(a)–(c) present the optimized monomers from various view angles; Table S1 lists the corresponding characterization data. The Cz-BD and Cz-DHBD COFs were synthesized through solvothermal method, the one-pot polycondensations of Cz-4CHO (Figs. S1–S7) and the benzidine derivatives BD and DHBD, respectively (Figs. S8–S13), in a mixture of dioxane and mesitylene (1:1) and the presence of acetic acid as a catalyst at 120 °C for 4 days (Scheme 1).

The resulting Cz-COFs were stable in air and were insoluble in organic solvents, including acetone, MeOH, tetrahydrofuran, *N*,*N*-dimethylformamide, dimethylsulfoxide, and dioxane. The success of the condensations of the Cz-COFs was validated using FTIR spectroscopy, solid state NMR spectroscopy, and elemental analysis. The FTIR spectrum of the monomer Cz-4CHO featured a characteristic signals at 1692 cm^{-1} for the aldehydic C═O group, at 2752 and 2845 cm^{-1} for the H–CO units, and at 3036 cm^{-1} for aromatic C–H stretching (Fig. 1(d)). The FTIR spectra of the Cz-BD and Cz-DHBD COFs featured strong peaks at 1615 and 1621 cm^{-1}, respectively, representing the C═N stretching vibrations, confirming the formation of imino linkages. Moreover, the signals of the NH_2 groups in the FTIR spectra of the diamine monomers near 3387–3205 cm^{-1} (Figs. S8 and 11) and of the C═O groups at 1692 cm^{-1} were strongly attenuated after the condensations, suggesting high degrees of polymerization (Fig. 1(d), S14, and S15). Although the spectra did feature trace signals for NH_2 and CHO groups, we presume them to represent unreacted terminal functional groups at the structural boundaries. The solid state NMR spectra featured two characteristic signals at 165 and 160 pm, revealing the imino bonds (C═N) of the Cz-BD and Cz-DHBD COFs, respectively (Fig. 1(e)). Thermogravimetric analysis (TGA) analyses confirmed the excellent thermal stabilities of these COFs. TGA revealed that Cz-COFs are thermally stable up to 450–500 °C in a Nitrogen atmosphere. Using temperature of 10% weight loss ($T_{d10\%}$) and char yield after heating at 800 °C as standards for thermal stability, we found that Cz-BD COF was characterized by a value of T_{d10} of 485 °C and a char yield of 55.8%. Similarly, the Cz-DHBD COF provided a value of T_{d10} of 507 °C with a residue of 53.3% (Fig. 2 and Table S2).

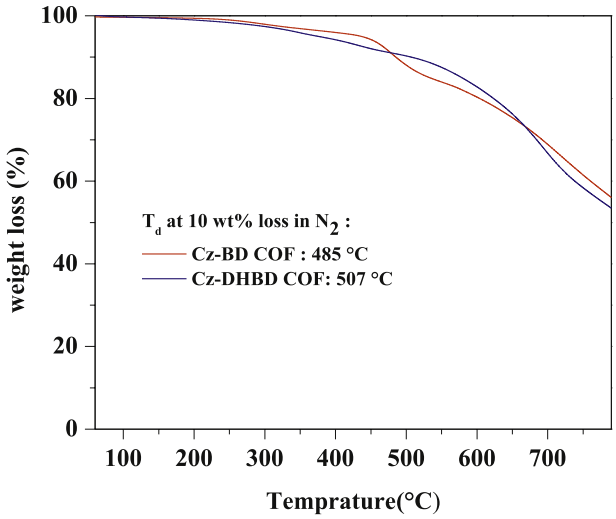

Fig. 2. TGA traces of the Cz-COFs, recorded under N_2 at a heating rate of 20 °C min^{-1}.

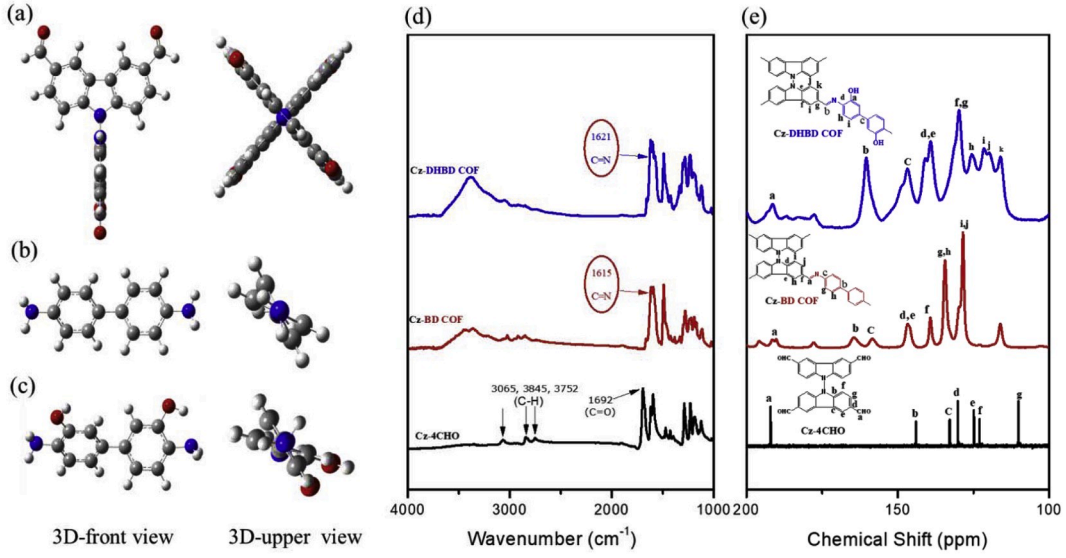

Fig. 1. (a–c) 3D-front and 3D-upper views of the monomers (a) Cz-4CHO, (b) BD, and (c) DHBD. (d) FTIR spectra of Cz-4CHO (black), Cz-BD COF (red), and Cz-DHBD COF (blue). (e) ^{13}C NMR spectrum of Cz-4CHO (black) and solid state ^{13}C NMR spectra of Cz-BD COF (red) and Cz-DHBD COF (blue).

Elemental analyses (Table S3) were consistent with the values calculated for 2D infinite sheets of both the Cz-BD and Cz-DHBD COFs. The matching of these results with the theoretical values reveals the good thermal stability of the Cz-COFs and the high residual ratio after high-temperature treatment. Also, as anticipated, both COFs possessed relatively high nitrogen atom contents (>9.9%), with the value for Cz-BD COF (10.99%) being higher than that for Cz-DHBD COF (9.91%).

3.2. Characterization of Cz-BD COF and Cz-HDBD COF

Powder X-ray diffraction (PXRD) revealed that both the Cz-BD and Cz-DHBD COFs possessed crystalline framework structures (Fig. 3). In the experimental PXRD data for Cz-BD COF, we attribute the strongest signals at 4.04 and 8.05° to the (110) and (220) facets, respectively; the signals at 12.11 and 5.75° to the (420) and (200) facets, respectively; and the broad signal at 22.15° to the (001) facets caused by π-stacking of the tetragonal COF layers (Fig. S16). Similarly, the PXRD pattern of the Cz-DHBD COF featured sharp peaks at 2.24 and 3.91° representing the (100) and (110) facets, respectively, and peaks at 8.19, 12.97, and 26.40° for the (200), (300), and (001) facets, respectively (Fig. S17). We calculated the average *d*-spacings between the 100 planes (d_{100}) by using the Bragg equation. The value of d_{100} for the Cz-BD COF was 2.1 nm, while the Cz-DHBD COF provided two values of 4.0 and 2.2 nm (Table S4). We also performed theoretical simulations of the PXRD patterns to determine the exact structural geometries of the obtained COFs. Here, Material Studio software was used to predict the PXRD patterns for the stacked structures and to match the simulated data with the experimental peak positions. Considering the possible crystalline structures of a single-pore-type COF (SP–COF) and a dual-pore-type COF (DP-COF), each structure was further divided into two possible packing models: eclipsed (AA) and staggered (AB). Pawley refinement for the single-pore-type structure was performed for the Cz-BD COF using a C222 space group with lattice parameters of $a = 23.606$ Å, $b = 23.108$ Å, and $c = 4.126$ Å for AA-stacking and with $c = 8.3$ Å for AB-stacking; this structure was the highest symmetry predicted from the DFT modeling, yielding a PXRD pattern that agreed with the experimental pattern with negligible differences. Dual-pore-type Pawley refinement was performed for the Cz-BD COF using a P6 space group with lattice parameters $a = 54.8$, $b = 54.8$, and $c = 4.8$ Å for AA-stacking and with $c = 9.6$ Å for AB-stacking, according to the DFT modeling. The resulting four packing models are defined herein as SP-AA-stacking, SP-AB-stacking, DP-AA-stacking, and DP-AB-stacking.

Comparison of the experimental PXRD data with the simulated pattern for the Cz-BD COF revealed a greater comparison with a SP-AA-stacking model (Fig. 3(a) and S18) with small difference evidenced by small R_{wp} (3.90%) and R_p (3.18%) values, suggesting that the Cz-BD COF possessed a tetragonal structure. In contrast, the Cz-DHBD COF provided a PXRD pattern identical with the simulated DP-AA-stacking pattern with neglectable differences revealed by small R_{wp} (4.04%) and R_p (3.09%) values, suggesting that the Cz-DHBD COF possessed a dual-pore-type structure, with one pore type having an hexagonal structure and the other a trigonal structure (Fig. 3(b) and S19). Thus, tetragonal SP-AA-stacking was more stable in the case of the Cz-BD COF, while hexagonal DP-AA-stacking was more stable than the orthorhombic structure in the case of the Cz-DHBD COF. In this context, both of the COFs exhibited their thermodynamically most stable configurations [25,29]. Notably, such a dual-pore-type structure was not been observed for COFs synthesized using monomers having the same symmetry ($C_2 + C_2$); only a single pore type was observed in that case [31]. We attribute this behavior to changes in the chemical structures of the monomers affecting the relative total energies of the resulting COFs and, hence, changing the topological structures of the synthesized COFs.

The N_2 adsorption/desorption isotherms and the pore size distributions supported the notion of the single- and dual-pore-type structures for these two COFs. In the isotherms of the two COFs, a sharp rise occurred at low relative pressure ($P/P_0 = 0.1$), followed by a slight increase at values of P/P_0 between 0.1 and 0.9, and then a sharp increase between 0.9 and 1.0. The two curves were type I isotherms, indicating that the two COFs possessed microporous characteristics (Fig. 4(a) and (b)). The Cz-BD and Cz-DHBD COFs exhibited maximum N_2 uptakes of 686.3 and 340.7 $m^2\ g^{-1}$, respectively, and possessed Brunauer–Emmett–Teller (BET) surface areas of 2111.0 and 992.2 $m^2\ g^{-1}$, respectively. In addition, the total pore volumes of these two COFs were 1.061 and 0.527 $cm^3\ g^{-1}$, respectively (Table S4). The porosities were

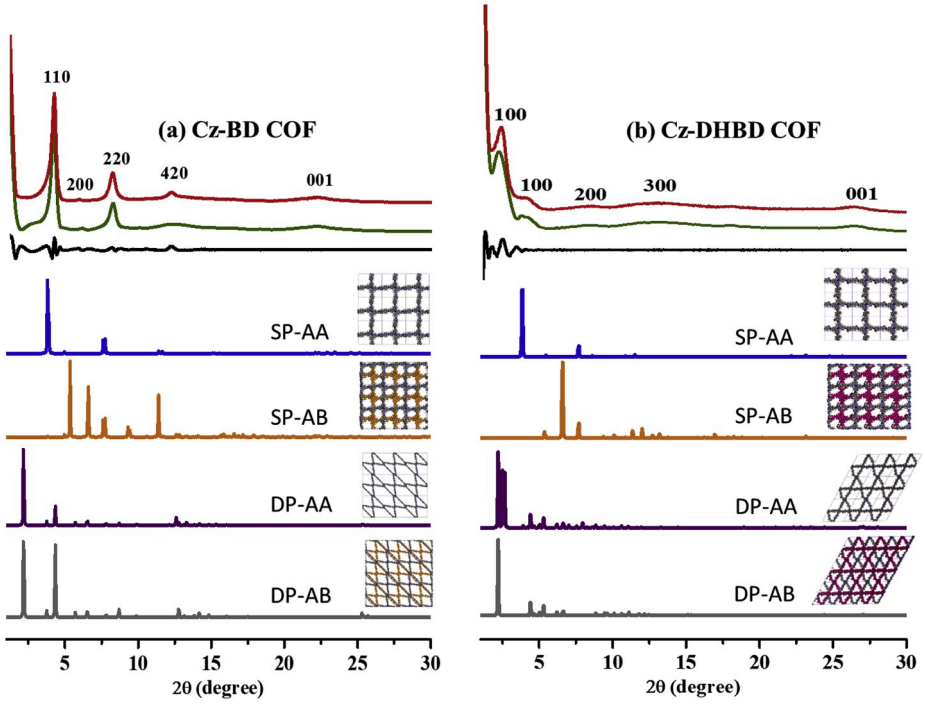

Fig. 3. PXRD profiles of (a) Cz-BD and (b) Cz-DHBD COFs: experimentally observed (red); Pawley-refined (green); difference between simulated and calculated data (black); simulated for the SP-AA (blue), SP-AB (orange), DP-AA (purple), and DP-AB (gray) stacking models.

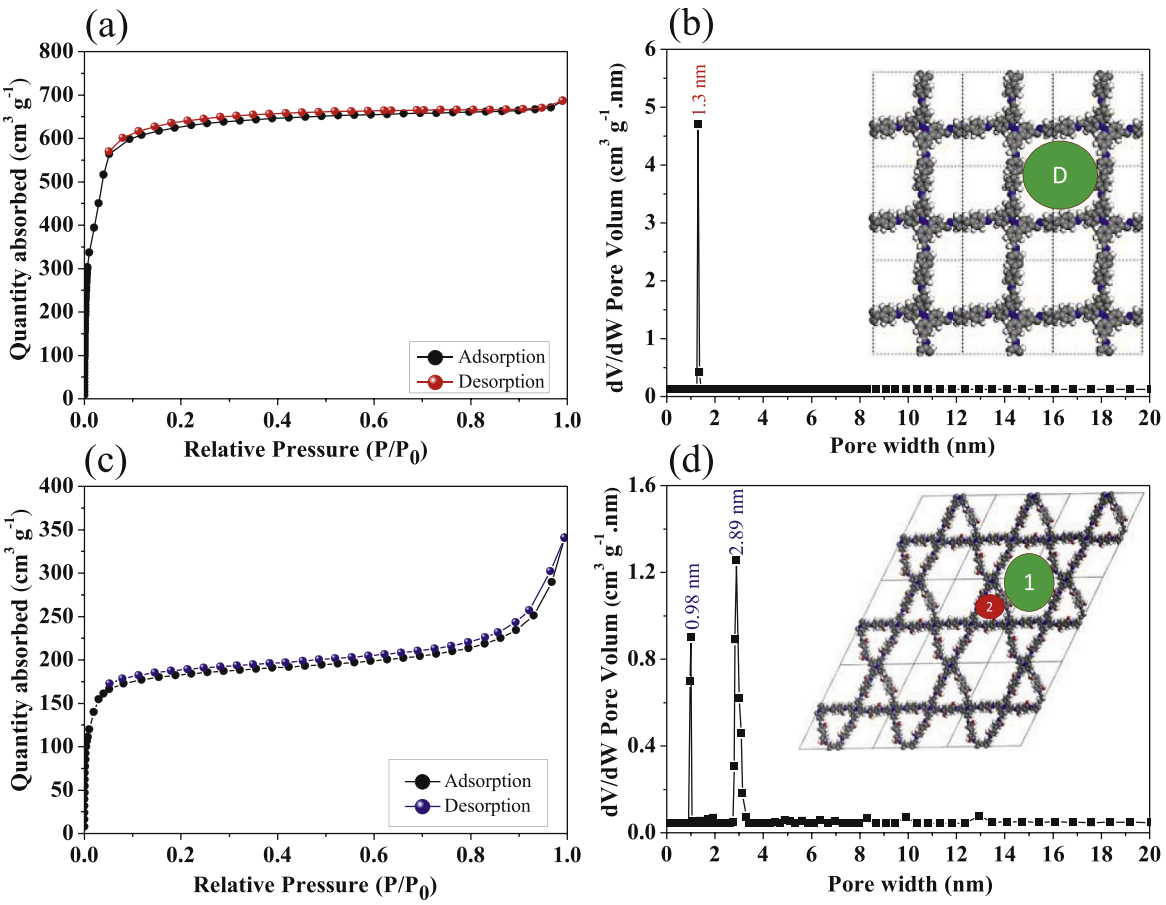

Fig. 4. (a, b) N_2 adsorption/desorption isotherms (measured at 77 K), (c, d) pore size distributions (calculated using NLDFT).

further investigated from pore-size distribution curves fitted using nonlocal density functional theory (NL-DFT). The pore size distributions were consistent with the PXRD simulated data and validated the single-porosity and dual-porosity characteristics of the Cz-BD and Cz-DHBD COFs, respectively. The Cz-BD COF featured a single pore size of 1.3 nm, while the Cz-DHBD COF featured two narrow pore sizes of 0.98 and 2.89 nm, which we assign to trigonal (microporous) and hexagonal (mesoporous) structures, respectively (Fig. 4(c) and (d)). Thus, the Cz-BD COF had a single pore size, whereas the Cz-DHBD COF exhibited a dual-pore-type (Kagome) structure.

We used field-emission scanning electron microscopy (FESEM) to investigate the morphologies of the Cz-BD and Cz-DHBD COFs. As displayed in Fig. 5(a) and (b), and S20, the FESEM images of the Cz-BD COF revealed an assembly of plate-like blocks, whereas those for the Cz-DHBD COF revealed an assembly of dark homogenous rods. In addition, transmission electron microscopy (TEM) images of the Cz-BD and Cz-DHBD COFs (Fig. 5(c) and (d), and S21) revealed the presence of porous networks, with those of the Cz-DHBD COF confirming the homogenous dark nature of the COF rods as well as the presence of porous networks in the Cz-DHBD COF backbone.

We examined the degrees of CO_2 adsorption of both COFs at temperatures of 298 and 273 K (Fig. 6(a) and (b)). The nucleophilicity of the nitrogen atoms in COFs plays a vital role affecting their CO_2 uptake capacity. Both the Cz-BD and Cz-DHBD COFs displayed excellent CO_2 uptake capacities compared to other porous materials (Table S5), with the Cz-BD COF providing values of 65.26 and 125.95 mg g^{-1} at 298 and 273 K, respectively, and the Cz-DHBD COF providing values of 57.28 and 110.59 mg g^{-1}, respectively. The slightly greater CO_2 uptake efficiencies of the Cz-BD COF relative to those of the Cz-DHBD COF were presumably due intramolecular hydrogen bonding of the OH groups in the Cz-DHBD units and the nitrogen atoms in the Schiff base units; the greater steric hindrance and lower nucleophilicity of the imino nitrogen atoms were responsible for the lower amount of adsorbed CO_2 [17,39]. In addition, we calculated the isosteric heats of adsorption (Q_{st}) for the Cz-BD and Cz-DHBD COFs, based on the Clausius–Clapeyron equation and their CO_2 adsorptions at 298 and 273 K (Fig. 6(c)). At approximately 0.1 mmol g^{-1}, the values of Q_{st} of the Cz-BD and Cz-DHBD COFs were 27.8 and 26.1 K J mol^{-1}, respectively. These values confirmed that intramolecular hydrogen bonding in the Cz-DHBD COF decreased the nucleophilicity of the imino nitrogen atoms and, thus, slightly decreases the number of adsorbed CO_2 molecules.

4. Conclusions

We have investigated the effect of using monomers of the same geometry (C_2 + C_2), but different structures, on the topologies of their resulting COFs. The prepared Cz-BD and Cz-DHBD COFs were thermally stable at temperatures up to 507 °C, and had large surface areas of 2111 and 992.2 m^2 g^{-1}, respectively. Both of these COFs were highly crystalline, with sharp XRD peaks; simulated data revealed that the Cz-BD and Cz-DHBD COFs possessed single- and dual-pore-type (Kagome) structures, respectively, the latter induced by intramolecular hydrogen bonding of OH···N units. The Cz-BD and CB-DHBD COFs possessed high affinity for CO_2 uptake: at 65.26 and 57.28 mg g^{-1}, respectively, at 298 K and 125.95 and 110.59 mg g^{-1}, respectively, at 273 K.

Declaration of competing interest

The authors declare that they have no known competing financial interests or personal relationships that could have appeared to influence

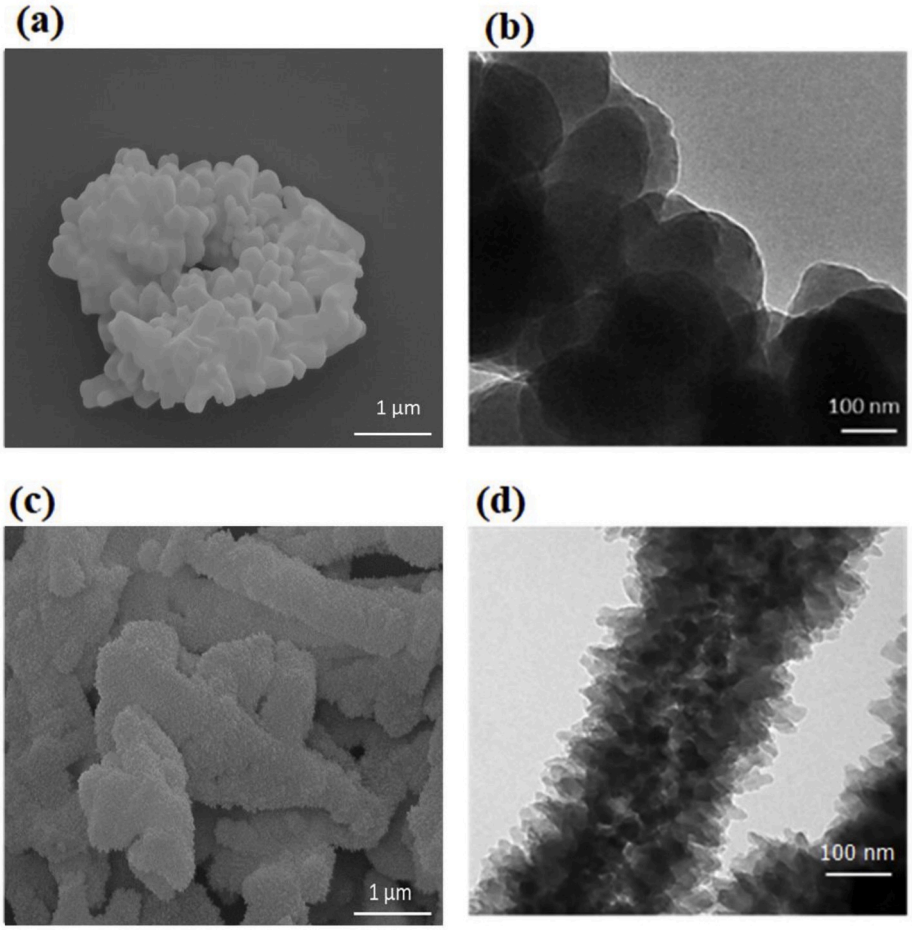

Fig. 5. (a, c) FE-SEM images, and (b, d) TEM images for the (a,b) Cz-BD and (c, d) Cz-DHBD COFs.

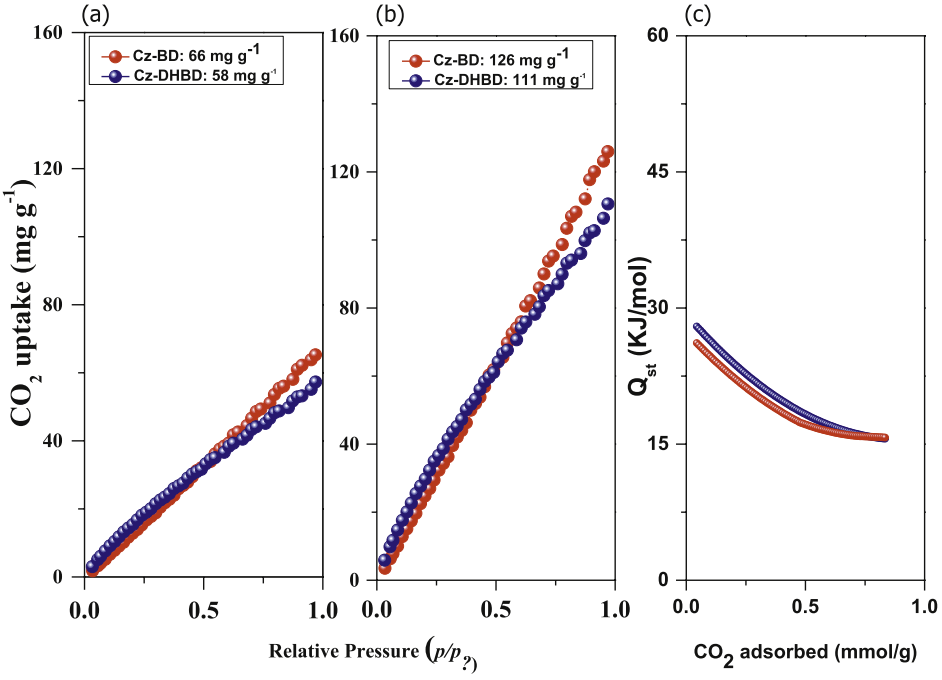

Fig. 6. (a, b) CO_2 uptake profiles of the Cz-BD and Cz-DHBD COFs at (a) 298 and (b) 273 K. (c) Values of Q_{st}.

the work reported in this paper.

CRediT authorship contribution statement

Hesham R. Abuzeid: Writing - original draft. **Ahmed F.M. EL-Mahdy:** Writing - original draft, Methodology. **Shiao-Wei Kuo:** Formal analysis, Writing - original draft, Writing - review & editing.

Acknowledgements

This study was supported financially by the Ministry of Science and Technology, Taiwan, under contracts MOST 106-2221-E-110-067-MY3, 108-2638-E-002-003-MY2, and 108-2221-E-110-014-MY3.

Appendix A. Supplementary data

Supplementary data to this article can be found online at https://doi.org/10.1016/j.micromeso.2020.110151.

References

[1] A.P. Cote, M.O. Keeffe, N.W. Ockwig, A.J. Matzger, O.M. Yaghi, Porous, crystalline, covalent organic frameworks, Science 310 (2005) 1166–1171.
[2] Y.V. Kaneti, S. Dutta, M.S.A. Hossain, M.J.A. Shiddiky, K.L. Tung, F.K. Shieh, C. K. Tsung, K.C.W. Wu, Y. Yamauchi, Strategies for improving the functionality of zeolitic imidazolate frameworks: tailoring nanoarchitectures for functional applications, Adv. Mater. 29 (2017), 1700213.
[3] Y.C. Sue, J.W. Wu, S.E. Chung, C.H. Kang, K.L. Tung, K.C.W. Wu, F.K. Shieh, Synthesis of hierarchical micro/mesoporous structures via solid-aqueous interface growth: zeolitic imidazolate framework-8 on siliceous mesocellular foams for enhanced pervaporation of water/ethanol mixtures, ACS Appl. Mater. Interfaces 6 (2014) 5192–5198.
[4] F.K. Shieh, S.C. Wang, C.I. Yen, C.C. Wu, S. Dutta, L.Y. Chou, J.V. Morabito, P. Hu, M.H. Hsu, K.C.W. Wu, C.K. Tsung, Imparting functionality to biocatalysts via embedding enzymes into nanoporous materials by a de Novo approach: size-selective sheltering of catalase in metal-organic framework microcrystals, J. Am. Chem. Soc. 137 (2015) 4276–4279.
[5] Y. Kuwahara, H. Kango, H. Yamashita, Catalytic transfer hydrogenation of biomass-derived levulinic acid and its esters to γ-valerolactone over sulfonic acid-functionalized UiO-66, ACS Sustain. Chem. Eng. 5 (2017) 1141–1152.
[6] Z.F. Pang, T.Y. Zhou, R.R. Liang, Q.Y. Qi, X. Zhao, Regulating the topology of 2D covalent organic frameworks by the rational introduction of substituents, Chem. Sci. 8 (2017) 3866–3870.
[7] C.S. Diercks, O.M. Yaghi, The atom, the molecule, and the covalent organic framework, Science 355 (2017), eaal1585.
[8] A.F.M. EL-Mahdy, Y.H. Hung, T.H. Mansoure, H.H.K.W.C. Wu, S.W. Kuo, Synthesis of [3+3] β-ketoenamine-tethered covalent organic frameworks (COFs) for high-performance supercapacitance and CO2 storage, J. Taiwan Inst. Chem. Eng. 103 (2019) 199–208.
[9] H.R. Abuzeid, A.F.M. El-Mahdy, M.M.M. Ahmed, S.W. Kuo, Triazine-functionalized covalent benzoxazine framework for direct synthesis of N-doped microporous carbon, Polym. Chem. 10 (2019) 6010–6020.
[10] A.F.M. EL-Mahdy, C. Young, J. Kim, J. You, Y. Yamauchi, S.W. Kuo, Hollow microspherical and microtubular [3 + 3] carbazole-based covalent organic frameworks and their gas and energy storage applications, ACS Appl. Mater. Interfaces 11 (2019) 9343–9354.
[11] A.F.M. EL-Mahdy, M.G. Mohamed, T.H. Mansoure, H.H. Yu, T. Chen, S.W. Kuo, Ultrastable tetraphenyl-p-phenylenediamine-based covalent organic frameworks as platforms for high-performance electrochemical supercapacitors, Chem. Commun. 55 (2019) 14890–14893.
[12] C. Wu, Y. Liu, H. Liu, C. Duan, Q. Pan, J. Zhu, F. Hu, X. Ma, T. Jiu, Z. Li, Y. Zhao, Highly conjugated three-dimensional covalent organic frameworks based on spirobifluorene for perovskite solar cell enhancement, J. Am. Chem. Soc. 140 (2018) 10016–10024.
[13] S. Yan, X. Guan, H. Li, D. Li, M. Xue, Y. Yan, V. Valtchev, S. Qiu, Q. Fang, Three-dimensional salphen-based covalent–organic frameworks as catalytic antioxidants, J. Am. Chem. Soc. 141 (2019) 2920–2924.
[14] H. Xu, S. Tao, D. Jiang, Proton conduction in crystalline and porous covalent organic frameworks, Nat. Mater. 15 (2016) 22–726.
[15] F.-Z. Cui, J.-J. Xie, S.-Y. Jiang, S.-X. Gan, D.-L. Ma, R.-R. Liang, G.-F. Jiang, X. Zhao, A gaseous hydrogen chloride chemosensor based on a 2D covalent organic framework, Chem. Commun. 55 (2019) 4550–4553.
[16] S. Wan, J. Guo, J. Kim, H. Ihee, D. Jiang, A belt-shaped, blue luminescent, and semiconducting covalent organic framework, Angew. Chem. Int. Ed. 47 (2008) 8826–8830.
[17] A.F.M. El-Mahdy, C.-H. Kuo, A.A. Alshehri, J. Kim, C. Young, Y. Yamauchi, S.-W. Kuo, Strategic Design of triphenylamine- and triphenyltriazine-based two-dimensional covalent organic frameworks for CO2 uptake and energy storage, J. Mater. Chem. 6 (2018) 19532–19541.
[18] A.F.M. El-Mahdy, Y.-H. Hung, T.H. Mansoure, H.-H. Yu, T. Chen, S.-W. Kuo, A hollow microtubular triazine- and benzobisoxazole-based covalent organic framework presenting sponge-like shells that functions as a high-performance supercapacitor, Chem. Asian J. 14 (2019) 1429–1435.
[19] A.P. Côté, H.M. El-Kaderi, H. Furukawa, J.R. Hunt, O.M. Yaghi, Reticular synthesis of microporous and mesoporous 2D covalent organic frameworks, J. Am. Chem. Soc. 129 (2007) 12914–12915.
[20] E.L. Spitler, B.T. Koo, J.L. Novotney, J.W. Colson, F.J. Uribe-Romo, G.D. Gutierrez, P. Clancy, W.R. Dichtel, A 2D covalent organic framework with 4.7-nm pores and insight into its interlayer stacking, J. Am. Chem. Soc. 133 (2011) 19416–19421.
[21] Q. Fang, Z. Zhuang, S. Gu, R.B. Kaspar, J. Zheng, J. Wang, S. Qiu, Y. Yan, Designed synthesis of large-pore crystalline polyimide covalent organic frameworks, Nat. Commun. 5 (2014) 4503.
[22] L.A. Baldwin, J.W. Crowe, M.D. Shannon, C.P. Jaroniec, P.L. McGrier, 2D covalent organic frameworks with alternating triangular and hexagonal pores, Chem. Mater. 27 (2015) 6169–6172.
[23] N. Huang, L. Zhai, D.E. Coupry, M.A. Addicoat, K. Okushita, K. Nishimura, T. Heine, D. Jiang, Multiple-component covalent organic frameworks, Nat. Commun. 7 (2016) 1–12.
[24] S. Kanti Das, S. Mishra, K. Manna, U. Kayal, S. Mahapatra, K. Das Saha, S. Dalapati, G.P. Das, A.A. Mostafa, A. Bhaumik, A new triazine based π-conjugated mesoporous 2D covalent organic framework: its *in vitro* anticancer activities, Chem. Commun. 54 (2018) 11475–11478.
[25] J.-X. Ma, J. Li, Y.-F. Chen, R. Ning, Y.-F. Ao, J.-M. Liu, J. Sun, D.-X. Wang, Q.-Q. Wang, Cage based crystalline covalent organic frameworks, J. Am. Chem. Soc. 141 (2019) 3843–3848.
[26] T. Zhou, S. Xu, Q. Wen, Z. Pang, X. Zhao, One-step construction of two di ff erent kinds of pores in a 2D covalent organic framework, J. Am. Chem. Soc. 136 (2014) 15885–15888.
[27] Y. Tian, S.Q. Xu, C. Qian, Z.F. Pang, G.F. Jiang, X. Zhao, Two-dimensional dual-pore covalent organic frameworks obtained from the combination of two: D2hsymmetrical building blocks, Chem. Commun. 52 (2016) 11704–11707.
[28] S. Dalapati, E. Jin, M. Addicoat, T. Heine, D. Jiang, Highly emissive covalent organic frameworks, J. Am. Chem. Soc. 138 (2016) 5797–5800.
[29] Q. Sun, B. Aguila, P.C. Lan, S. Ma, Tuning pore heterogeneity in covalent organic frameworks for enhanced enzyme accessibility and resistance against denaturants, Adv. Mater. (2019), 1900008.
[30] Z.F. Pang, T.Y. Zhou, R.R. Liang, Q.Y. Qi, X. Zhao, Regulating the topology of 2D covalent organic frameworks by the rational introduction of substituents, Chem. Sci. 8 (2017) 3866–3870.
[31] S. Dalapati, S. Jin, J. Gao, Y. Xu, A. Nagai, D. Jiang, An azine-linked covalent organic framework, J. Am. Chem. Soc. 135 (2013) 17310–17313.
[32] X. Chen, N. Huang, J. Gao, H. Xu, F. Xu, D. Jiang, Towards covalent organic frameworks with predesignable and aligned open docking sites, Chem. Commun. 50 (2014) 6161–6163.
[33] S. Feng, H. Xu, C. Zhang, Y. Chen, J. Zeng, D. Jiang, J.-X. Jiang, Bicarbazole-based redox-active covalent organic frameworks for ultrahigh-performance energy storage, Chem. Commun. 53 (2017) 11334–11337.
[34] Z.-F. Pang, S.-Q. Xu, T.-Y. Zhou, R.-R. Liang, T.-G. Zhan, X. Zhao, Construction of covalent organic frameworks bearing three different kinds of pores through the heterostructural mixed linker strategy, J. Am. Chem. Soc. 138 (2016) 4710–4713.
[35] Y. Zhu, S. Wan, Y. Jin, W. Zhang, Desymmetrized vertex Design for the synthesis of covalent organic frameworks with periodically heterogeneous pore structures, J. Am. Chem. Soc. 137 (2015) 13772–13775.
[36] L. Ascherl, T. Sick, J.T. Margraf, S.H. Lapidus, M. Calik, C. Hettstedt, K. Karaghiosoff, M. Döblinger, T. Clark, K.W. Chapman, et al., Molecular docking sites designed for the generation of highly crystalline covalent organic frameworks, Nat. Chem. 8 (2016) 310–316.
[37] S. Kandambeth, D.B. Shinde, M.K. Panda, B. Lukose, T. Heine, R. Banerjee, Enhancement of chemical stability and crystallinity in porphyrin-containing covalent organic frameworks by intramolecular hydrogen bonds, Angew. Chem. Int. Ed. 52 (2013) 13052–13056.
[38] N. Huang, P. Wang, D. Jiang, Covalent organic frameworks: a materials platform for structural and functional designs, Nat. Rev. Mater. 1 (2016) 16068.
[39] P.V. Kortunov, M. Siskin, M. Paccagnini, H. Thomann, CO_2 reaction mechanisms with hindered alkanolamines: control and promotion of reaction pathways, Energy Fuels 30 (2016) 1223–1236.